On the Compactness, Efficiency, and Representation of 3D Convolutional Networks: Brain Parcellation as a Pretext Task

Wenqi Li, Guotai Wang, Lucas Fidon, Sebastien Ourselin, M. Jorge Cardoso, and Tom Vercauteren

Translational Imaging Group, Centre for Medical Image Computing (CMIC),
University College London, London, UK
Wellcome/EPSRC Centre for Surgical and Interventional Science, University College
London, London, UK

Abstract. Deep convolutional neural networks are powerful tools for learning visual representations from images. However, designing efficient deep architectures to analyse volumetric medical images remains challenging. This work investigates efficient and flexible elements of modern convolutional networks such as dilated convolution and residual connection. With these essential building blocks, we propose a high-resolution, compact convolutional network for volumetric image segmentation. To illustrate its efficiency of learning 3D representation from large-scale image data, the proposed network is validated with the challenging task of parcellating 155 neuroanatomical structures from brain MR images. Our experiments show that the proposed network architecture compares favourably with state-of-the-art volumetric segmentation networks while being an order of magnitude more compact. We consider the brain parcellation task as a pretext task for volumetric image segmentation; our trained network potentially provides a good starting point for transfer learning. Additionally, we show the feasibility of voxel-level uncertainty estimation using a sampling approximation through dropout.

1 Introduction

Convolutional neural networks (CNNs) have been shown to be powerful tools for learning visual representations from images. They often consist of multiple layers of non-linear functions with a large number of trainable parameters. Hierarchical features can be obtained by training the CNNs discriminatively.

In the medical image computing domain, recent years have seen a growing number of applications using CNNs. Although there have been recent advances in tailoring CNNs to analyse volumetric images, most of the work to date studies image representations in 2D. While volumetric representations are more informative, the number of voxels scales cubically with the size of the region of interest. This raises challenges of learning more complex visual patterns as well as higher computational burden compared to the 2D cases. While developing compact and

effective 3D network architectures is of significant interest, designing 3D CNNs remains a challenging problem.

The goal of this paper is to design a high-resolution and compact network architecture for the segmentation of fine structures in volumetric images. For this purpose, we study the simple and flexible elements of modern convolutional networks, such as dilated convolution and residual connection. Most of the existing network architectures follow a fully convolutional downsample-upsample pathway [11,4,15,3,16,13]. Low-level features with high spatial resolutions are first downsampled for higher-level feature abstraction; then the feature maps are upsampled to achieve high-resolution segmentation. In contrast to these, we propose a novel 3D architecture that incorporates high spatial resolution feature maps throughout the layers, and can be trained with a wide range of receptive fields. We validate our network with the challenging task of automated brain parcellation into 155 structures from T1-weighted MR images. We show that the proposed network, with twenty times fewer parameters, achieves competitive segmentation performance compared with state-of-the-art architectures.

A well-designed network could be trained with a large-scale dataset and enables transfer learning to other image recognition tasks [9]. In the field of computer vision, the well-known AlexNet and VGG net were trained on the ImageNet dataset. They provide general-purpose image representations that can be adapted for a wide range of computer vision problems. Given the large amount of data and the complex visual patterns of the brain parcellation problem, we consider it as a pretext task. Our trained network is the first step towards a general-purpose volumetric image representation. It potentially provides an initial model for transfer learning of other volumetric image segmentation tasks.

The uncertainty of the segmentation is also important for indicating the confidence and reliability of one algorithm [5,18,19]. The high uncertainty of labelling can be a sign of an unreliable classification. In this work, we demonstrate the feasibility of voxel-level uncertainty estimation using Monte Carlo samples of the proposed network with dropout at test time. Compared to the existing volumetric segmentation networks, our compact network has fewer parameter interactions, and thus potentially achieves better uncertainty estimates with fewer samples.

2   On the elements of 3D convolutional networks

Convolutions and dilated convolutions. To maintain a relatively low number of parameters, we choose to use small 3D convolutional kernels with only 3^3 parameters for all convolutions. This is about the smallest kernel that can represent 3D features in all directions with respect to the central voxel. Although a convolutional kernel with $5 \times 5 \times 5$ voxels gives the same receptive field as stacking two layers of $3 \times 3 \times 3$-voxel convolution, the latter has approximately 57% fewer parameters. Using smaller kernels implicitly imposes more regularisation on the network while achieving the same receptive field.

To further enlarge the receptive field to capture large image contexts, most of the existing volumetric segmentation networks downsample the intermediate feature maps. This significantly reduces the spatial resolution. For example, 3D U-net [3] heavily employs $2 \times 2 \times 2$-voxel max pooling with strides of two voxels in each dimension. Each max pooling reduces the feature responses of the previous layer to only 1/8 of its spatial resolution. Upsampling layers, such as deconvolutions, are often used subsequently to partially recover the high resolution of the input. However, adding deconvolution layers also introduces additional computational costs.

Recently, Chen et al. [2] used dilated convolutions with upsampled kernels for semantic image segmentation. The advantages of dilated convolutions are that the features can be computed with a high spatial resolution, and the size of the receptive field can be enlarged arbitrarily. Dilated convolutions can be used to produce accurate dense predictions and detailed segmentation maps along object boundaries.

In contrast to the downsample-upsample pathway, we propose to adopt dilated convolutions for volumetric image segmentation. More specifically, the convolutional kernels are upsampled with a dilation factor r. For M-channels of input feature maps $\mathbf{I}$, the output feature channel $\mathbf{O}$ generated with dilated convolutions are:

$$\mathbf{O}_{x,y,z} = \sum_{m=0}^{M-1} \sum_{i=0}^{2} \sum_{j=0}^{2} \sum_{k=0}^{2} \mathbf{w}_{i,j,k,m} \mathbf{I}_{(x+ir),(y+jr),(z+kr),m} \; ; \tag{1}$$

where the index tuple (x, y, z) runs through every spatial location in the volumes; the kernels $\mathbf{w}$ consist of $3^3 \times M$ trainable parameters. The dilated convolution in Eq. (1) has the same number of trainable parameters as the standard $3 \times 3 \times 3$ convolution. It preserves the spatial resolution and provides a $(2r + 1)^3$-voxel receptive field. Setting r to 1 reduces the dilated convolution to the standard $3 \times 3 \times 3$ convolution. In practice, we implement 3D dilated convolutions with a split-and-merge strategy [2] to benefit from the existing GPU convolution routines.

Residual connections. Residual connections were first introduced and later refined by He et al. [7,8] for the effective training of deep networks. The key idea of residual connection is to create identity mapping connections to bypass the parameterised layers in a network. The input of a residual block is directly merged to the output by addition. The residual connections have been shown to make information propagation smooth and improve the training speed [7].

Fig. 1. A block with residual connections.

More specifically, let the input to the p-th layer of a residual block as $\mathbf{x}_p$, the output of the block $\mathbf{x}_{p+1}$ has the form: $\mathbf{x}_{p+1} = \mathbf{x}_p + F(\mathbf{x}_p, \mathbf{w}_p)$; where $F(\mathbf{x}_p, \mathbf{w}_p)$
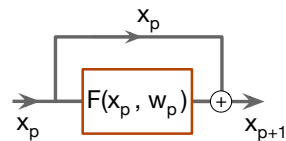
denotes the path with non-linear functions in the block (shown in Fig. 1). If we stack the residual blocks, the last layer output $\mathbf{x}_l$ can be expressed as: $\mathbf{x}_l = \mathbf{x}_p + \sum_{i=p}^{l-1} F(\mathbf{x}_i, \mathbf{w}_i)$. The residual connections enables direct information propagation from any residual block to another in both forward pass and back-propagation.

Effective receptive field. One interpretation of the residual network is that they behave like ensembles of relatively shallow networks. The unravelled view of the residual connections proposed by Veit et al. [20] suggests that the networks with n residual blocks have a collection of 2^n unique paths.

Without residual connections, the receptive field of a network is generally considered fixed. However, when training with n residual blocks, the networks utilise 2^n different paths and therefore features can be learned with a large range of different receptive fields. For example, the proposed network with 9 residual blocks (see Section 3) has a maximum receptive field of $87 \times 87 \times 87$ voxels. Following the unravel view of the residual network, it consists of 2^9 unique paths. Fig. 2 shows the distribution of the receptive field of these paths. The receptive fields range from $3 \times 3 \times 3$ to $87 \times 87 \times 87$, following a binomial distribution.

This differs from the existing 3D networks. For example, Deepmedic [11] model operates at two paths, with a fixed receptive field $17 \times 17 \times 17$ and $42 \times 42 \times 42$ respectively. 3D U-net [3] has a relatively large receptive field of about $88 \times 88 \times 88$ voxels. However, there are only eight unique paths and receptive fields.

Fig. 2. Histogram of the receptive fields.

Intuitively, given that the receptive field of a deep convolutional network is relatively large, the segmentation maps will suffer from distortions due to the border effects of convolution. That is, the segmentation results near the border of the output volume are less accurate due to the lack of input supporting window. We conduct experiments and demonstrate that the proposed networks generate only a small distortion near the borders (See Section 4). This suggests training the network with residual connections reduces the effective receptive field. The width of the distorted border is much smaller than the maximum receptive field. This phenomenon was also recently analysed by Luo et al. [14]. In practice, at test time we pad each input volume with a border of zeros and discard the same amount of border in the segmentation output.
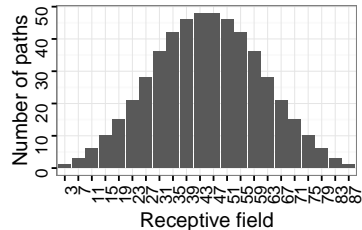
Loss function. The last layer of the network is a softmax function that gives scores over all labels for each voxel. Typically, the end-to-end training procedure minimises the cross entropy loss function using an N-voxel image volume $\{x_n\}_{n=1}^{N}$ and the training data of C-class segmentation map $\{y_n\}_{n=1}^{N}$ where

$y_n \in \{1, \ldots, C\}$ is:

$$\mathcal{L}(\{x_n\}, \{y_n\}) = -\frac{1}{N} \sum_{n=1}^{N} \sum_{c=1}^{C} \delta(y_n = c) \log F_c(x_n), \tag{2}$$

where δ corresponds to the Dirac delta function, $F_c(x_n)$ is the softmax classification score of x_n over the c-th class. However, when the training data are severely unbalanced (which is typical in medical image segmentation problems), this formulation leads to a strongly biased estimation towards the majority class. Instead of directly re-weighting each voxel by class frequencies, Milletari et al. [16] propose a solution by maximising the mean Dice coefficient directly, i.e.,

$$\mathcal{D}(\{x_n\}, \{y_n\}) = \frac{1}{C} \sum_{c=1}^{C} \frac{2 \sum_{n=1}^{N} \delta(y_n = c) F_c(x_n)}{\sum_{n=1}^{N} [\delta(y_n = c)]^2 + \sum_{n=1}^{N} [F_c(x_n)]^2}. \tag{3}$$

We employ this formulation to handle the issue of training data imbalance.

Uncertainty estimation using dropout. Gal and Ghahramani demonstrated that the deep network trained with dropout can be cast as a Bayesian approximation of the Gaussian process [5]. Given a set of training data and their labels $\{\mathbf{X}, \mathbf{Y}\}$, training a network $F(\cdot, \mathbf{W})$ with dropout has the effect of approximating the posterior distribution $p(\mathbf{W}|\{\mathbf{X}, \mathbf{Y}\})$ by minimising the Kullback-Leibler divergence term, i.e. $\mathrm{KL}(q(\mathbf{W})\|p(\mathbf{W}|\{\mathbf{X}, \mathbf{Y}\}))$; where $q(\mathbf{W})$ is an approximating distribution over the weight matrices $\mathbf{W}$ with their elements randomly set to zero according to Bernoulli random variables. After training the network, the predictive distribution of test data $\hat{\mathbf{x}}$ can be expressed as $q(\hat{\mathbf{y}}|\hat{\mathbf{x}}) = \int F(\hat{\mathbf{x}}, \mathbf{W}) q(\mathbf{W}) d\mathbf{W}$. The prediction can be approximated using Monte Carlo samples of the trained network: $\hat{\mathbf{y}} = \frac{1}{M} \sum_{m=1}^{M} F(\hat{\mathbf{x}}, \mathbf{W}_m)$, where $\{\mathbf{W}_m\}_{m=1}^{M}$ is a set of M samples from $q(\mathbf{W})$. The uncertainty of the prediction can be estimated using the sample variance of the M samples.

With this theoretical insight, we are able to estimate the uncertainty of the segmentation map at the voxel level. We extend the segmentation network with a $1 \times 1 \times 1$ convolutional layer before the last convolutional layer. The extended network is trained with a dropout ratio of 0.5 applied to the newly inserted layer. At test time, we sample the network N times using dropout. The final segmentation is obtained by majority voting. The percentage of samples which disagrees with the voting results is calculated at each voxel as the uncertainty estimates.

3   The network architecture and its implementation

3.1   The proposed architecture

Our network consists of 20 layers of convolutions. In the first seven convolutional layers, we adopt $3 \times 3 \times 3$-voxel convolutions. These layers are designed
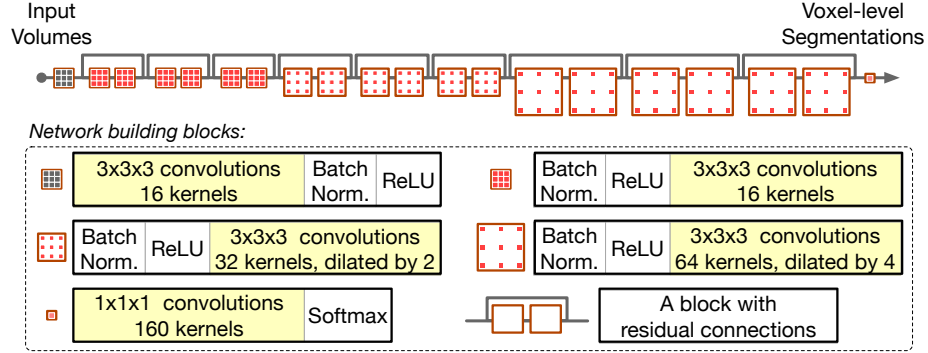
Fig. 3. The proposed network architecture for volumetric image segmentation. The network mainly utilises dilated convolutions and residual connections to make an end-to-end mapping from image volume to a voxel-level dense segmentation. To incorporate features at multiple scales, the dilation factor of the dilated convolutions is gradually increased when the layer goes deeper. The residual blocks with identity mapping enable the direct fusion of features from different scales. The spatial resolution of the input volume is maintained throughout the network.

to capture low-level image features such as edges and corners. In the subsequent convolutional layers, the kernels are dilated by a factor of two or four. These deeper layers with dilated kernels encode mid- and high-level image features.

Residual connections are employed to group every two convolutional layers. Within each residual block, each convolutional layer is associated with an element-wise rectified linear unit (ReLU) layer and a batch normalisation layer [10]. The ReLU, batch normalisation, and convolutional layers are arranged in the pre-activation order [8].

The network can be trained end-to-end. In the training stage, the inputs to our network are $96 \times 96 \times 96$-voxel images. The final softmax layer gives classification scores over the class labels for each of the $96 \times 96 \times 96$ voxels. The architecture is illustrated in Fig. 3.

3.2   Implementation details

In the training stage, the pre-processing step involved input data standardisation and augmentation at both image- and subvolume-level. At image-level, we adopted the histogram-based scale standardisation method [17] to normalised the intensity histograms. As a data augmentation at image-level, randomisation was introduced in the normalisation process by randomly choosing a threshold of foreground between the volume minimum and mean intensity (at test time, the mean intensity of the test volume was used as the threshold). Each image was further normalised to have zero mean and unit standard deviation. Augmentations on the randomly sampled $96 \times 96 \times 96$ subvolumes were employed on the fly. These included rotation with a random angle in the range of $[-10°, 10°]$ for

each of the three orthogonal planes and spatial rescaling with a random scaling factor in the range of $[0.9, 1.1]$.

All the parameters in the convolutional layers were initialised according to He et al. [6]. The scaling and shifting parameters in the batch normalisation layers were initialised to 1 and 0 respectively. The networks were trained with two Nvidia K80 GPUs. At each training iteration, each GPU processed one input volume; the average gradients computed over these two training volumes were used as the gradients update. To make a fair comparison, we employed the Adam optimisation method [12] for all the methods with fixed hyper-parameters. The learning rate lr was set to 0.01, the step size hyper-parameter β_1 was 0.9 and β_2 was 0.999 in all cases, except V-Net for which we chose the largest lr that the training algorithm converges ($lr = 0.0001$). The models were trained until we observed a plateau in performance on the validation set. We do not employ additional spatial smoothing function (such as conditional random field) as a post-processing step. Instead of aiming for better segmentation results by adding post-processing steps, we focused on the dense segmentation maps generated by the networks. As we consider brain parcellation as a pretext task, networks without explicit spatial smoothing are potentially more reusable. We implemented all the methods (including a re-implementation of Deepmedic [11], V-net [16], and 3D U-net [3] architecture) with Tensorflow[1].

4   Experiments and results

Data. To demonstrate the feasibility of learning complex 3D image representations from large-scale data, the proposed network is learning a highly granular segmentation of 543 T1-weighted MR images of healthy controls from the ADNI dataset. The average number of voxels of each volume is about $182 \times 244 \times 246$. The average voxel size is approximately $1.18mm \times 1.05mm \times 1.05mm$. All volumes are bias-corrected and reoriented to a standard Right-Anterior-Superior orientation. The bronze standard parcellation of 155 brain structures and 5 non-brain outer tissues are obtained using the GIF framework [1]. Fig. 5(left) shows the label distribution of the dataset. We randomly choose 443, 50, and 50 volumes for training, test, and validation respectively.

Overall evaluation. In this section, we compare the proposed high-resolution compact network architecture (illustrated in Fig. 3; denoted as *HC-default*) with three variants: (1) the HC-default configuration without the residual connections, trained with cross-entropy loss function (*NoRes-entropy*); (2) the HC-default configuration without residual connections, trained with Dice loss function (*NoRes-dice*); and (3) the HC-default configuration trained with an additional dropout layer, and makes predictions with a majority voting of 10 Monte Carlo samples (*HC-dropout*). For the dropout variant, our dropout layer employed before the last convolutional layer consists of 80 kernels.

---

[1] The source code is available at `https://github.com/gift-surg/HighRes3DNet`
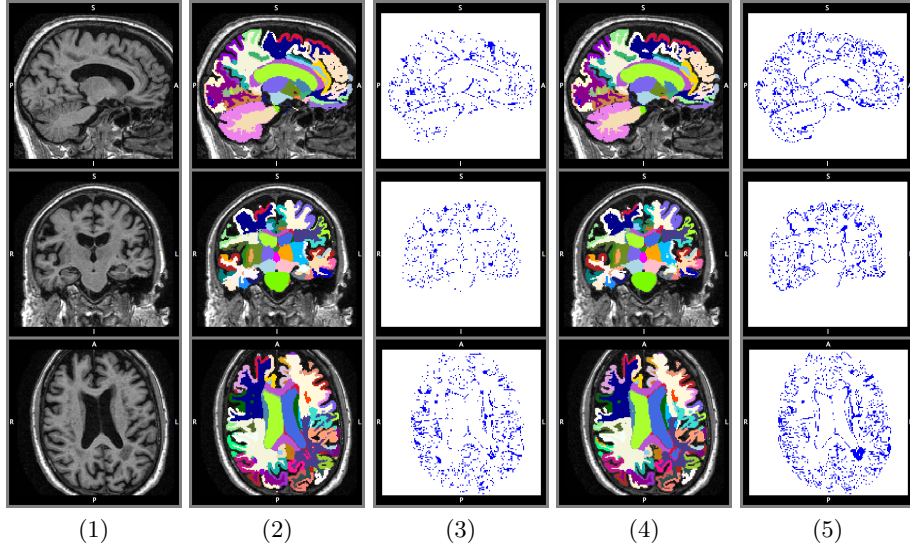
Fig. 4. Visualisations of segmentation results. (1) slices from a test image volume, segmentation maps and false prediction maps generated by HC-dropout (2, 3), and 3D U-net-dice (4, 5).

Table 1. Comparison of different 3D convolutional network architectures.

Architecture	Multi-layer fusion	Num. param.	Loss type	DCS (%)	STD (%)
HC-default	Residual	0.81M	Dice loss	82.05	2.96
HC-dropout	Residual	0.82M	Dice loss	**84.34**	**1.89**
NoRes-entropy	N/A	0.81M	Cross entr.	39.36	1.13
NoRes-dice	N/A	0.81M	Dice loss	75.47	2.97
Deepmedic[11]-dice	Two pathways	0.68M	Dice loss	78.74	1.72
3D U-net[3]-dice	Feature forwarding	19.08M	Dice loss	80.18	6.18
V-net[16]	Feature forwarding	62.63M	Dice loss	74.58	1.86

Additionally, three state-of-the-art volumetric segmentation networks are evaluated. These include 3D U-net [3], V-net [16], and Deepmedic [11]. The last layer of each network architecture is replaced with a 160-way softmax classifier.

We observe that training these networks with the cross entropy loss function (Eq. 2) leads to poor segmentation results. Since the cross-entropy loss function treats all training voxels equally, the network may have difficulties in learning representations related to the minority classes. Training with the Dice loss function alleviates this issue by implicitly re-weighting the voxels. Thus we train all networks using the Dice loss function for a fair comparison.

We use the mean Dice Coefficient Similarity (DCS) as the performance measure. Table 1 and Fig. 5(right) compare the performance on the test set. In terms of our network variants, the results show that the use of Dice loss function largely improves the segmentation performance. This suggests that the Dice loss
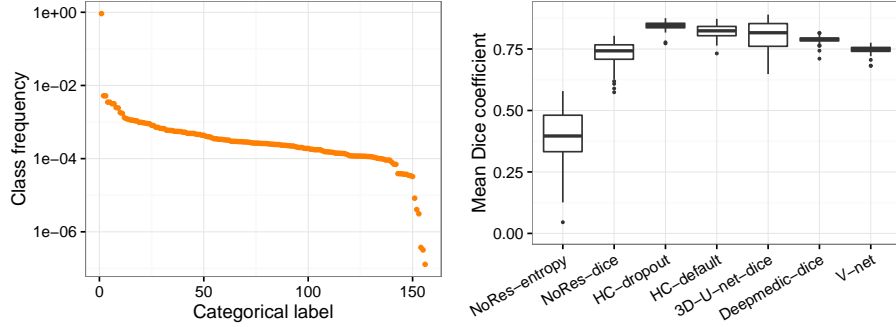
Fig. 5. Left: label distribution of the dataset; right: comparison of different network architectures.
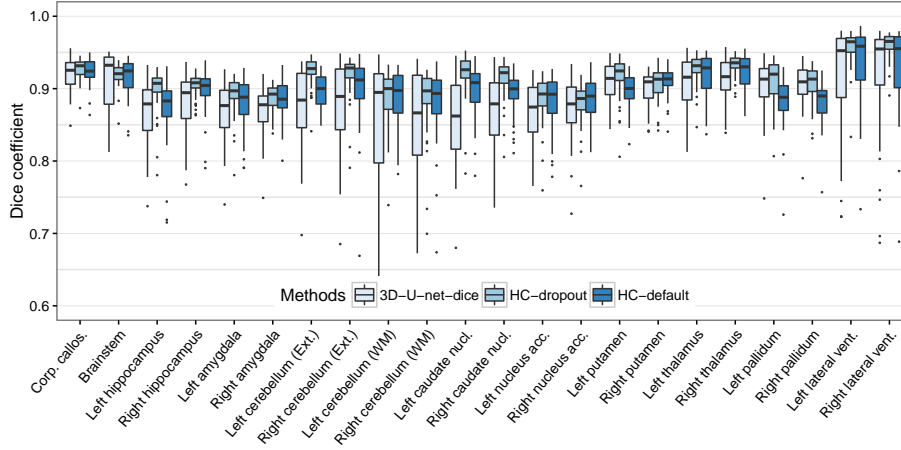

Fig. 6. Segmentation performance against a set of key structures.

function can handle the severely unbalanced segmentation problem well. The results also suggest that introducing the residual connections improved the segmentation performance measured in mean DCS. This indicates that the residual connections are important elements of the proposed network. By adopting the dropout method, the DCS can be further improved by 2% in DCS.

With a relatively small number of parameters, our HC-default and HC-dropout outperform the competing methods in terms of mean DCS. This suggests that our network is more effective for the brain parcellation problem. Note that V-net has a similar architecture to 3D U-net and has more parameters, but does not employ the batch normalisation technique. The lower DCS produced by V-net suggests that batch normalisation is important for training the networks for brain parcellation.

In Fig. 6, we show that the dropout variant achieves better segmentation results for all the key structures. Fig. 4 presents an example of the segmentation results of the proposed network and 3D U-net-Dice.

Receptive field and border effects. We further compare the segmentation performance of a trained network by discarding the borders in each dimension of the segmentation map. That is, given a $d \times d \times d$-voxel input, at border size 1 we only preserve the $(d-2)^3$-voxel output volume centred within the predicted map. Fig. 7 plots the DCS and standard errors of segmentation according to the size of the segmentation borders in each dimension. The results show that the distorted border is around 17 voxels in each dimension. The border effects do not severely decrease the segmentation performance. In practice, we pad the volume images with 16 zeros in each dimension, and remove the same amount of borders in the segmentation output.
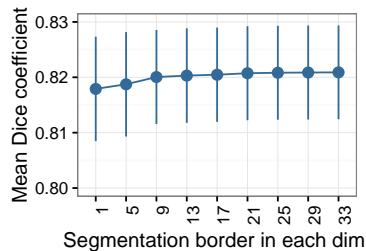

Fig. 7. Empirical analysis of the segmentation borders. Voxels near to the volume borders are classified less accurately.

The effect of number of samples in uncertainty estimations. This section investigates the number of Monte Carlo samples and the segmentation performance of the proposed network. Fig. 8(a) suggests that using 10 samples is enough to achieve good segmentation. Further increasing the number of samples has relatively small effects on the DCS. Fig. 8(b) plots the voxel-wise segmentation accuracy computed using only the voxels with an uncertainty less than a threshold. The voxel-wise accuracy is high when the threshold is small. This indicates that the uncertainty
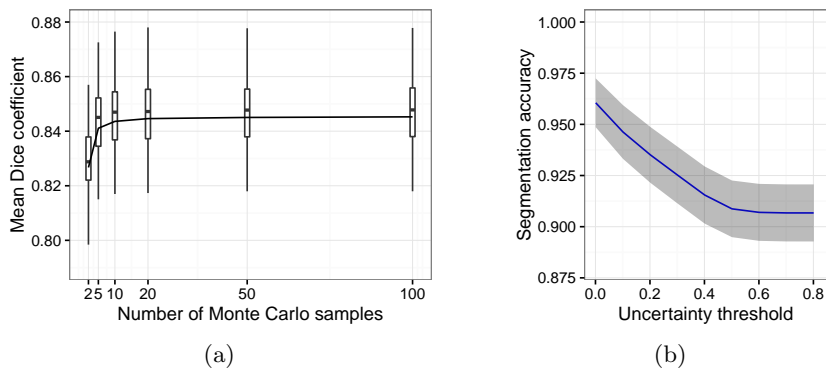

(a)   (b)

Fig. 8. Evaluation of dropout sampling. (a) The segmentation performance against the number of Monte Carlo samples. (b) voxel-level segmentation accuracy by thresholding the uncertainties. The shaded area represents the standard errors.
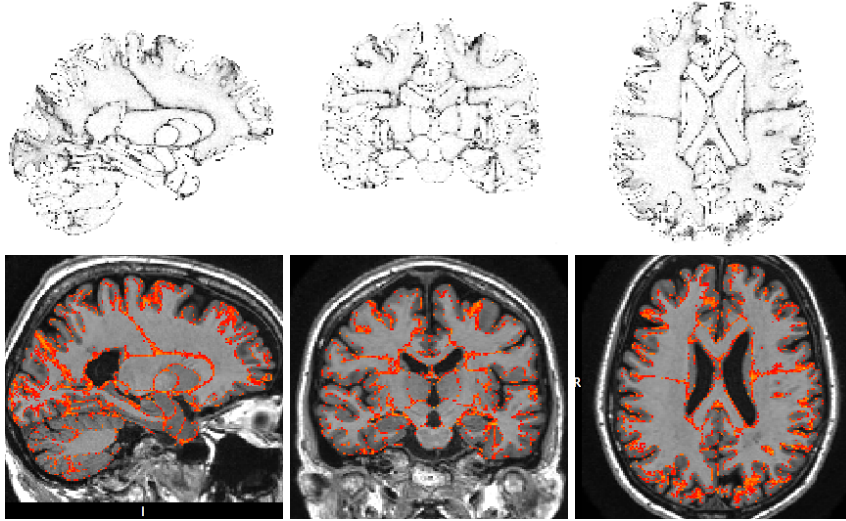
Fig. 9. Voxel-level segmentation uncertainty estimations. Top row: uncertainty map generated with 100 Monte Carlo samples using dropout. Bottom row: uncertainty map thresholded at 0.1.

estimation reflects the confidence of the network. Fig. 9 shows an uncertainty map generated by the proposed network. The uncertainties near the boundaries of different structures are relatively higher than the other regions.

Currently, our method takes about 60 seconds to predict a typical volume with $192 \times 256 \times 256$ voxels. To achieve better segmentation results and measure uncertainty, 10 Monte Carlo samples of our dropout model are required. The entire process takes slightly more than 10 minutes in total. However, during the Monte Carlo sampling at test time, only the dropout layer and the final prediction layer are randomised. To further reduce the computational time, the future software could reuse the features extracted from the layers before dropout, resulting in only a marginal increase in runtime when compared to a single prediction.

5   Conclusion

In this paper, we propose a high-resolution, 3D convolutional network architecture that incorporates large volumetric context using dilated convolutions and residual connections. Our network is conceptually simpler and more compact than the state-of-the-art volumetric segmentation networks. We validate the proposed network using the challenging task of brain parcellation in MR images. We show that the segmentation performance of our network compares favourably with the competing methods. Additionally, we demonstrate that Monte Carlo sampling of dropout technique can be used to generate voxel-level uncertainty es-

timation for our brain parcellation network. Moreover, we consider the brain parcellation task as a pretext task for volumetric image segmentation. Our trained network potentially provides a good starting point for transfer learning of other segmentation tasks.

In the future, we will extensively test the generalisation ability of the network to brain MR scans obtained with various scanning protocols from different data centres. Furthermore, we note that the uncertainty estimations are not probabilities. We will investigate the calibration of the uncertainty scores to provide reliable probability estimations.

References

1. Cardoso, M.J., Modat, M., Wolz, R., Melbourne, A., Cash, D., Rueckert, D., Ourselin, S.: Geodesic information flows: Spatially-variant graphs and their application to segmentation and fusion. IEEE Transactions on Medical Imaging 34(9) (2015)
2. Chen, L.C., Papandreou, G., Kokkinos, I., Murphy, K., Yuille, A.L.: DeepLab: Semantic image segmentation with deep convolutional nets, atrous convolution, and fully connected CRFs. arXiv:1606.00915 (2016)
3. Çiçek, Ö., Abdulkadir, A., Lienkamp, S.S., Brox, T., Ronneberger, O.: 3D U-Net: Learning dense volumetric segmentation from sparse annotation. In: MICCAI (2016)
4. Dou, Q., Chen, H., Yu, L., Zhao, L., Qin, J., Wang, D., Mok, V.C., Shi, L., Heng, P.A.: Automatic detection of cerebral microbleeds from MR images via 3D convolutional neural networks. IEEE Transactions on Medical Imaging 35(5) (2016)
5. Gal, Y., Ghahramani, Z.: Dropout as a Bayesian approximation: Representing model uncertainty in deep learning. In: ICML (2016)
6. He, K., Zhang, X., Ren, S., Sun, J.: Delving deep into rectifiers: Surpassing human-level performance on imagenet classification. In: ICCV (2015)
7. He, K., Zhang, X., Ren, S., Sun, J.: Deep residual learning for image recognition. In: CVPR (2016)
8. He, K., Zhang, X., Ren, S., Sun, J.: Identity mappings in deep residual networks. In: ECCV (2016)

9. Huh, M., Agrawal, P., Efros, A.A.: What makes ImageNet good for transfer learning? arXiv:1608.08614 (2016)
10. Ioffe, S., Szegedy, C.: Batch normalization: Accelerating deep network training by reducing internal covariate shift. In: ICML (2015)
11. Kamnitsas, K., Ledig, C., Newcombe, V.F., Simpson, J.P., Kane, A.D., Menon, D.K., Rueckert, D., Glocker, B.: Efficient multi-scale 3D CNN with fully connected CRF for accurate brain lesion segmentation. Medical Image Analysis 36 (2017)
12. Kingma, D., Ba, J.: Adam: A method for stochastic optimization. arXiv:1412.6980 (2014)
13. Kleesiek, J., Urban, G., Hubert, A., Schwarz, D., Maier-Hein, K., Bendszus, M., Biller, A.: Deep MRI brain extraction: A 3D convolutional neural network for skull stripping. NeuroImage 129 (2016)
14. Luo, W., Li, Y., Urtasun, R., Zemel, R.: Understanding the effective receptive field in deep convolutional neural networks. In: NIPS (2016)
15. Merkow, J., Kriegman, D., Marsden, A., Tu, Z.: Dense volume-to-volume vascular boundary detection. In: MICCAI (2016)
16. Milletari, F., Navab, N., Ahmadi, S.A.: V-Net: Fully convolutional neural networks for volumetric medical image segmentation. In: International Conference on 3D Vision (2016)
17. Nyúl, L.G., Udupa, J.K., Zhang, X.: New variants of a method of MRI scale standardization. IEEE Transactions on Medical Imaging 19(2) (2000)
18. Sankaran, S., Grady, L.J., Taylor, C.A.: Real-time sensitivity analysis of blood flow simulations to lumen segmentation uncertainty. In: MICCAI (2014)
19. Shi, W., Zhuang, X., Wolz, R., Simon, D., Tung, K., Wang, H., Ourselin, S., Edwards, P., Razavi, R., Rueckert, D.: A multi-image graph cut approach for cardiac image segmentation and uncertainty estimation. In: International Workshop on Statistical Atlases and Computational Models of the Heart (2011)
20. Veit, A., Wilber, M., Belongie, S.: Residual networks are exponential ensembles of relatively shallow networks. In: NIPS (2016)